Materials and Structures (2021) 54:26
https://doi.org/10.1617/s11527-021-01622-z

ORIGINAL ARTICLE

Characterization of mechanical behavior and mechanism of hybrid fiber reinforced cementitious composites after exposure to high temperatures

Deming Zeng · Mingli Cao · Xing Ming

Received: 22 July 2020 / Accepted: 5 January 2021 / Published online: 20 January 2021

Abstract In this paper, we developed a novel hybrid fiber reinforced cementitious composites (HFRCCs) using steel fibers, polyvinyl alcohol (PVA) fibers and calcium carbonate whisker (CW) with high temperature resistance and cost-effectiveness. Mechanical and physical responses of HFRCCs after exposure to high temperature and roles of different fibers were particularly studied. The results showed that partially replacing PVA fibers by CW could reduce the deterioration of strengths and flexural toughness of HFRCCs before 600 °C because of significant nucleation effect and restraining cracking of CW. PVA fibers would melt above 200 °C and thus deteriorated the flexural and splitting tensile strengths, but less effective to compressive strengths. Steel fiber was most effective to increase the residual mechanical properties among these fibers because of its higher thermostability and strong bond with matrix. Generally, high temperature deteriorated the matrix and adversely affected the quality of fibers, which was mainly related to the different thermostability between fibers.

Keywords Hybrid fiber · High temperature · Mechanical and physical properties · Calcium carbonate whisker

1 Introduction

Concrete, as a traditional cementitious composite, is widely used in many constructions because of its general availability and relatively low price [1]. Traditional cementitious composites are usually intrinsically brittle [2–4], so various fibers with different dimensions and properties are generally added into traditional cementitious composites to restrict the generation and propagation of cracks at different scales and stages, and thus to improve its toughness, ductility and further strength [5–8]. In recent years, incorporation of different single fibers and hybrid fibers have been tried and performed good enhancement and synergistic effect on mechanical properties of traditional cementitious composites [9–11]. Among these fibers widely used in cementitious composites, carbon nanotubes and carbon nanofibers caught researchers' attention because of their pronounced improvement at nano- and micro-

Supplementary Information The online version contains supplementary material available at https://doi.org/10.1617/s11527-021-01622-z.

D. Zeng · M. Cao (✉) · X. Ming
School of Civil Engineering, Dalian University of Technology, Dalian 116024, Liaoning, China
e-mail: minglic@dlut.edu.cn

D. Zeng
e-mail: zdm2429757869@163.com

X. Ming
e-mail: 13774034082@mail.dlut.edu.cn; 13774034082@163.com

scales [12–17]. However, the high-cost and agglomeration greatly limit their further use in developing ultra-high performance fiber reinforced cementitious composites [1, 3]. Therefore, to seek a kind of proper micro-fiber with high cost-effective and significant reinforcing effect to replace expensive fibers like carbon nanotubes and carbon nanofibers, and investigate the mechanical properties of concrete at ambient temperature and high temperature are valuable to develop high performance or ultra-high performance fiber reinforced cementitious composites.

Fire resistance research of a new building material is an important part of public protection and necessary for its large-scale use in construction projects, especially for developing ultra-high performance cementitious composites which usually demonstrates extensive cracking and spalling [18]. Elevated high temperatures would cause progressive damages on hydration products, which further accompanied with severe loss in strength and even durability, and finally cause the complete loss of bearing capacity of structures and buildings [19–21]. The mechanical properties and internal changes of cementitious composites with fibers after high temperature exposure were further investigated by numerous literatures. Therefore, it can be found the mechanical properties and microstructure of heated fiber reinforced cementitious composites will be significantly different from those at ambient temperature both from the fibers and matrix perspectives.

Literatures available showed that the needle-like CW with a length of 20–30 μm and a diameter of 1–2 μm as well as low price and excellent dispersion can be successfully used in cementitious composites to improve their flexural strength and cracking resistance [3, 22–24]. Also, it can demonstrate positive synergic effect in combination with other fibers (such as carbon fiber, steel fiber and PVA fiber) [3, 11]. Moreover, due to the thermostability and good cracking-resistance of CW at high temperature and lower price compared with PVA fibers, CW is certainly considered to partially replace steel fibers and PVA fibers in this study. The flexural strength, compressive strength, splitting tensile strength, mass loss and ultrasonic pulse velocity (UPV) of hybrid fiber (PVA-steel fiber, CW-PVA-steel fiber) cementitious composites after high temperature exposure (up to 900 °C) were tested. Besides, deterioration mechanism of high temperatures and fibers effects are discussed based on scanning electron microscope (SEM) observation.

2 Experimental procedure

2.1 Material and specimen preparation

P.O 42.5R ordinary Portland cement, CW and PVA fibers and quartz sand were used as the main raw materials. The chemical compositions of cement and CW are shown in Table 1. The mechanical parameters of fibers are shown in Table 2. The morphologies of CW are described in Fig. 1. In order to reduce the bubbles produced in the mix process, tributyl phosphate (TBP) was used as a defoamer in this experiment. Superplasticizer (Polycarboxylic acid type, ASTM C494 type F, water reducing ratio 24.1%) was added to ensure similar workability y of mixtures. The different mix proportions of raw materials were shown in Table 3. The water to cement ratio (*w/c*) and sand to cement ratio (*s/c*) was constant equal to 0.3 and 0.5, respectively. The productive processes of the mixture were presented in Fig. 2. The mixture was cast into a plastic mold with a dimension of 40 mm × 40 mm × 160 mm and vibrated for 60 s. After 24 h of curing in a cement/concrete standard curing box, the specimens were demoulded and cured in water at 20 °C for 28 days until they were tested.

2.2 Heating regimes

All of the specimens were placed in an oven to dry surface water for at least 24 h after the curing period. Thereafter, these specimens were put into an electric furnace and exposed to 200 °C, 400 °C, 500 °C, 600 °C, 800 °C, 900 °C, respectively at a heating rate of 3 °C/min. In order to form a stable thermal temperature field within the specimens, these target temperatures were maintained for 2 h. Then the furnace was turned off and specimens were cooled down to the ambient temperature in the furnace.

2.3 Test methods

Mechanical tests were performed before and after high temperature exposure. For the flexural strength test, a computer-controlled electrohydraulic servo universal equipment was employed at a displacement rate of

Table 1 Chemical constituents of cement and CW

Constituent	CaO	SiO_2	Al_2O_3	Fe_2O_3	CO_2	MgO	K_2O	SO_3	Na_2O
Cement	61.13	21.45	5.24	2.89	2.37	2.08	0.81	2.50	0.77
CW	54.93	0.29	0.11	0.07	42.07	2.14	–	0.31	–

Table 2 Mechanical parameters of steel fiber, PVA fiber and whisker

Constituent	Length (mm)	Aspect ratio (l/d)	Tensile strength (MPa)	Elastic modulus (GPa)	Density (g/cm^3)
Steel fiber	13	65	2850	200–210	7.8
PVA fiber	6	151.1	1529.5	36.7	1.3
CW	0.02–0.03	10–60	3000–6000	410–710	2.86

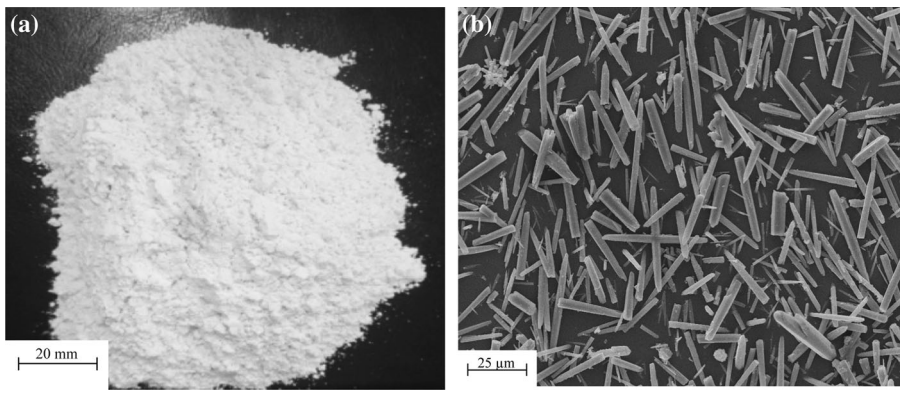

Fig. 1 Morphologies of CW at different scales; **a** macro morphology, **b** micro morphology

Table 3 Dosage of different fiber combinations by total volume fraction

Group	Volume fraction (%)			Fiber dosage (kg/m^3)		
	SF	PVA	CW	SF	PVA	CW
SP1	1.5	0.5	0	117	6.45	0
SPW1	1.5	0.4	1	117	5.16	28.6
SP2	1.25	0.75	0	97.5	9.68	0
SPW2	1.25	0.55	2	97.5	7.10	57.2

0.5 mm/min. The four-point bending test is shown in Fig. 3. Two opposite linear variable displacement transducers (LVDT) were used to measure the mid-span deflections of the beams. Compressive strength was determined by the two portions of prisms left after the flexural test. The compressive test and splitting tensile test were performed according to GB/T 50081-2002 [25] using the same machine as the bending test. Ultrasonic pulse velocity (UPV) test is directly associated with the porosity of specimens and the mass loss can show the decomposition of hydrates [26]. For the UPV test, TICO ultrasonic instrument, manufactured by Earth Products China Co. Ltd., was used. A pair of related transducers (transmitter and receiver) were located in the centre of the opposite sides of the prism in a direct transmission mode according to ASTM C597 and Chinese standard CECS 21:2000, as shown in Fig. 4 [27, 28].

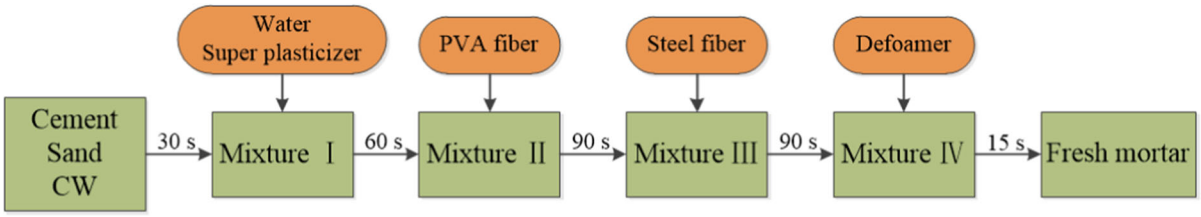

Fig. 2 Mix procedure for fresh cement paste mixtures

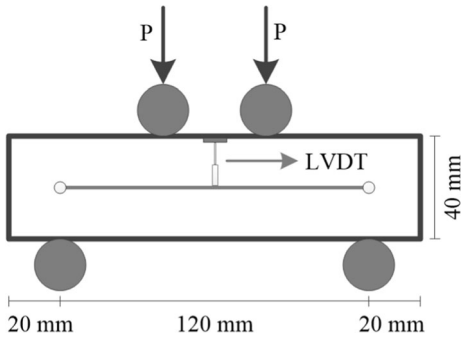

Fig. 3 Loading method of four-point bending test

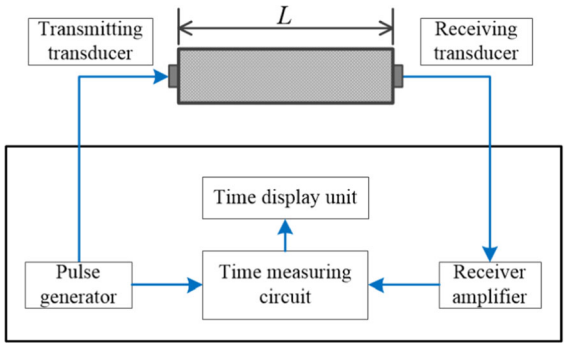

Fig. 4 Schematic of UPV testing

3 Results and discussion

3.1 Flexural strength and splitting tensile strength

The curves of relative residual flexural strength and splitting tensile strength versus temperature of four specimen groups are shown in Fig. 5. The value of relative residual strength is expressed by $f_{A,T}/f_A$, where f_A is the residual strength at ambient temperature, and $f_{A,T}$ is the residual strength of the specimens after exposure to different temperatures.

It can be seen in Fig. 5 that the relative residual flexural and splitting tensile strengths decreased below 200 °C, which was due to the evaporation of free water

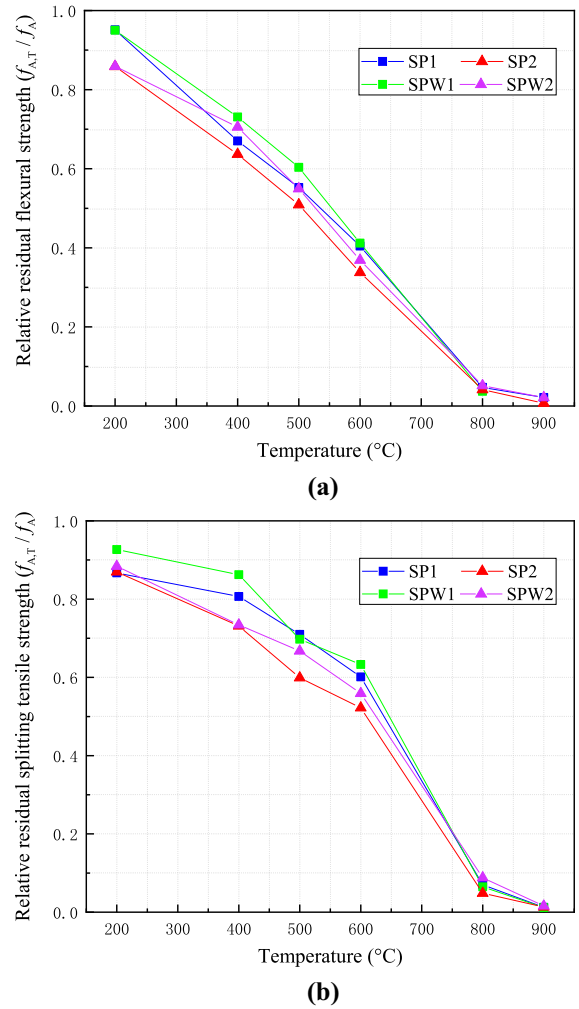

Fig. 5 Relative residual strengths of specimens after exposure to different temperatures; **a** relative residual flexural strength, **b** relative residual splitting tensile strength

in the capillary pores and dehydration of calcium silicate hydrate (C-S–H), ettringite (AFt) and monosulfoaluminate (AFm) [19]. Moreover, the relative residual flexural and splitting tensile strengths of SP2 and SPW2 were similar, which showed that SP2 and

SPW2 had the same degree of deterioration after exposure to 200 °C.

Between 200 and 600 °C, the relative residual flexural and splitting tensile strengths decreased further with the increase of temperature. One reason for this phenomenon was that the melting of PVA fibers. Above 200 °C, PVA fibers melt and left the channels in the matrix [10, 29, 30]. As a result, the fibers lost their ability to limit cracks development and the strength decreased. Also, the decomposition of $Ca(OH)_2$ between 400 and 500 °C further deteriorated the matrix [31–34].

Although the residual flexural and splitting tensile strength deteriorated with increase of temperature, the specimen containing CW generally had higher relative residual flexural and splitting tensile strength than those without CW after exposure to different temperatures, as can be seen in Fig. 5. It was mainly due to the reinforcing effect of CW before 600 °C [11, 26, 35]. In detail, CW could refine the distribution of pores, optimize the microstructure of the matrix at ambient temperature and restrain the cracking below 600 °C. In addition, the aragonite CW transferred to the calcite CW at about 375° C, where nucleation effect had a positive effect on the strength, producing C-S–H [36]. Also, the lower PVA fiber content of SPW1 and SPW2 was favorable to reduce the deterioration of flexural strengths and splitting tensile strengths.

Above 600 °C, the flexural strengths and splitting tensile strengths pronouncedly decreased with increase of temperature because of decomposition of $CaCO_3$ and C–S–H [19, 21, 37, 38]. It could be found that SP1 had higher relative residual flexural and splitting tensile strength than SPW1 but SP2 had lower relative values than SPW2 in this temperature range. Although CW completely decomposed above 800 °C and deteriorated the strengths and microstructure, the decomposition of CW could supply enough Ca solution for sintering process of aluminate phases, which might accelerate the generation of ceramic phases. Therefore, more studies should be conducted on this novel phenomenon in our further research.

It should also be noted the relative residual strength of SPW1 was higher than that of SPW2, and SP1 was higher than SP2 from ambient temperature to 900 °C, which meant that steel fibers were effective to reduce the deterioration of strengths because of its high thermostability. In general, the SPW1 demonstrated favorable response to high temperatures in terms of flexural strengths and splitting tensile strengths.

3.2 Compressive strength

Figure 6 represents the relative residual compressive strength after exposure to different temperatures. The residual compressive strengths decreased up to 200 °C. And specimens containing CW had higher relative compressive strengths than those without CW, which were similar to the responses of flexural and splitting tensile strengths. Between 200 and 400 °C, compressive strengths increased slightly, especially for SPW1 and SPW2. This might be that further hydration of unhydrated cement particles under hydrothermal condition and nucleation effect of calcite CW (transferred from aragonite CW) could compact the matrix and further improved the compressive strengths [11, 21, 36]. Although PVA fibers melt above 200 °C, this deterioration effect was dominant in flexural and splitting tensile strengths responses to elevated temperatures because of their higher sensitiveness to cracks induced by PVA fibers than compressive strengths. Above 400 °C, the residual compressive strength decreased, which was attributed to the decomposition of C–S–H, $Ca(OH)_2$, $CaCO_3$ [19, 21, 37, 38].

Similarly, steel fibers were effective to reduce the deterioration on compressive strengths and SPW1 performed better among all these groups in terms of residual and relative compressive strengths.

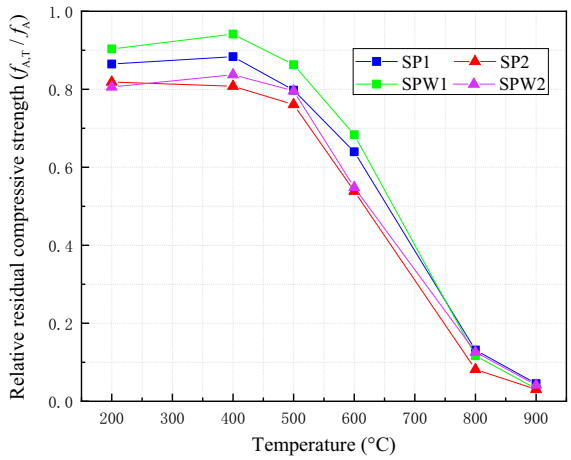

Fig. 6 Relative residual compressive strengths after exposure to different temperatures

3.3 Flexural load–deflection curves

The average load deflection curves based on the four-point bending test are shown in Fig. 7. These curves were obtained from at least three specimens by calculating average load corresponding to deflection since all the load responses were quite consistent in each series. Because HFRCCs severely lost their bearing capacity after exposed to 900 °C, only the load–deflection curves of HFRCCs from the ambient temperature to 800 °C are shown.

It can be seen both the peak load and the corresponded deflection (peak deflection) decreased roughly at elevated temperatures. Particularly, it can be seen that the load–deflection curves of HFRCCs performed certain hardening responses below 200 °C. Above 200 °C, the hardening behavior was not as obvious as that below 200 °C, which was attributed to the melting of PVA fibers induced by high temperatures [10, 29, 30]. Also, the post-peak softening branches obtained below 200 °C were obviously better than those obtained above 200 °C, which indicated that the melting of PVA fibers promoted the deterioration of the post-peak softening branch.

The energy absorption capacity of the fiber-reinforced cementitious composites under flexural load

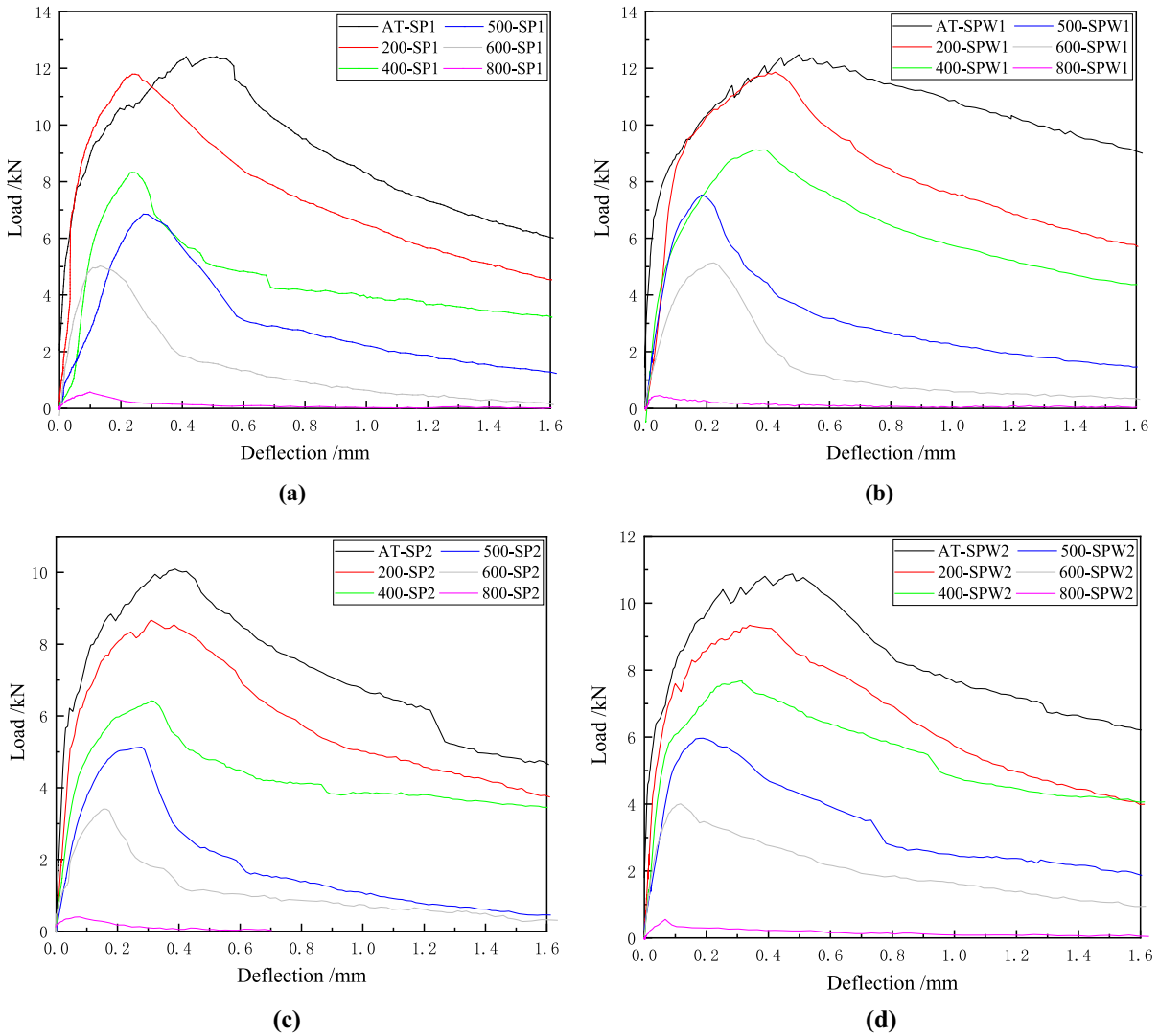

Fig. 7 Load–deflection curves of **a** SP1; **b** SPW1; **c** SP2; **d** SPW2 after exposure to elevated temperatures

can be evaluated by flexural toughness. It is measured by taking the area under the load–deflection curve up to a specific deflection, given by:

$$T_{\mathrm{b}} = \int_0^{\delta} P(\sigma)\mathrm{d}\sigma \tag{1}$$

where T_{b} is flexural toughness, N m; δ is specimen deflection and set as 1.2 mm (L/10 0) here; P(σ) is flexural load. The equivalent flexural strength for four points bending beam proposed by JCI-SF4 [39] is given as:

$$\sigma_b = \frac{T_{\mathrm{b}}}{\delta_{\mathrm{tb}}} \times \left(\frac{L}{b \times h^2}\right) \tag{2}$$

where σ_b is equivalent flexural strength, MPa; T_{b} is felxural toughness of the mortar up to a specified deflection of specimen; δ_{tb} is the specified deflection of mortar and set as 1.2 mm (L/100) here; L, b and h are the span, width and depth of the specimen, respectively.

The calculated flexural toughness and equivalent flexural strengths are presented in Figs. 8 and 9. It was obvious that flexural toughness and equivalent flexural strength decreased with the increase of temperature, which indicated that the energy absorption capacity of HFRCCs under external load was increasingly affected by temperature and the ability to bear external loads became weaker. There were three main reasons for the phenomena: (1) the deterioration of matrix caused by decomposition of hydrates; (2) the deterioration of fiber properties induced by high temperature; (3) the weakening bond strength between the fibers and the matrix [40]. The equivalent flexural strengths and flexural toughness of SP1 increased by 6–35% compared with that of SP2 after exposure to different temperatures. This showed that toughness of HFRCCs could be effectively improved through partially replacing PVA fibers by steel fibers because of high thermostability of steel fibers [10, 29, 30]. Besides, the equivalent flexural strengths and flexural toughness of SPW1 and SPW2 increased by 1–29% and 11–43% compared with those of SP1 and SP2, respectively. This indicated that the substitution of PVA fibers with CW was favorable to improve the toughness of HFRCCs to some extent because of reinforcing effect of CW before 600 °C [4, 11, 26].

3.4 UPV and mass loss rate

The UPV test is a nondestructive testing (NDT) method that can reflect the internal defects and pores of matrix through the change of UPV. In general, UPV will increase when there are less internal defects and pores. Figure 10 represents relative UPV of HFRCCs after exposure to different temperatures. Where U_{A} is the residual UPV at ambient temperature, and $U_{\mathrm{A,T}}$ is the residual UPV of the specimens after exposure to high temperatures.

It can be seen that relative UPV decreased from 200 to 900 °C, which meant more defects and pores had generated by decomposition of hydrates and melting of PVA fibers. Particularly, SP2 with the highest PVA fiber content had the lowest relative UPV after exposed to high temperature from 400 to 600 °C. The relative UPV of SPW2 was the highest, which demonstrated that the addition of CW was beneficial to fill and refine the pores in concrete matrix even

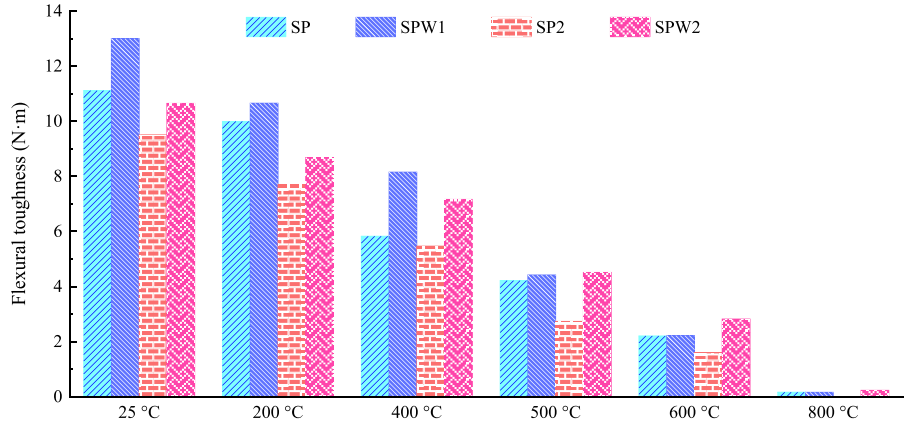

Fig. 8 Flexural toughness of specimens after exposure to elevated temperatures

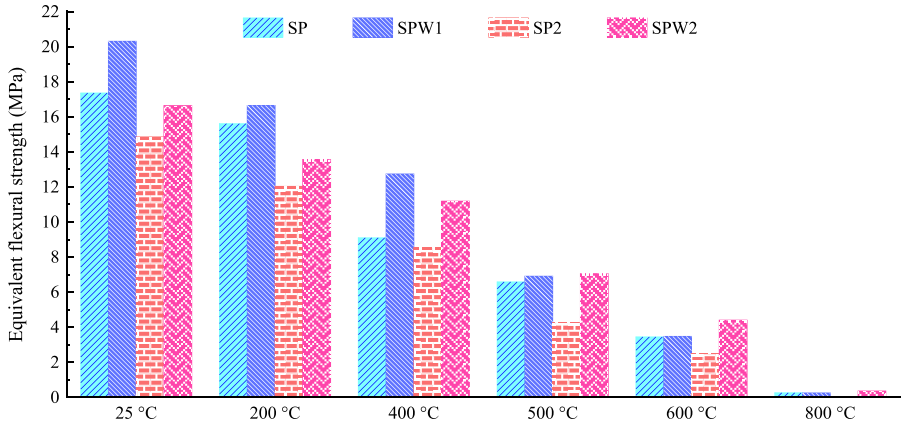

Fig. 9 Equivalent flexural strength of specimens after exposure to elevated temperatures

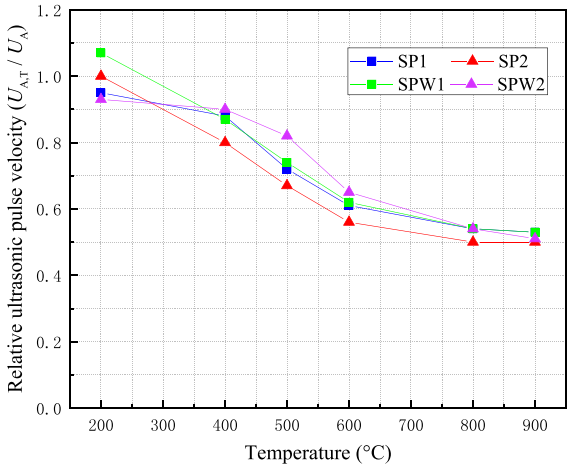

Fig. 10 Relative ultrasonic pulse velocity after exposure to different temperatures

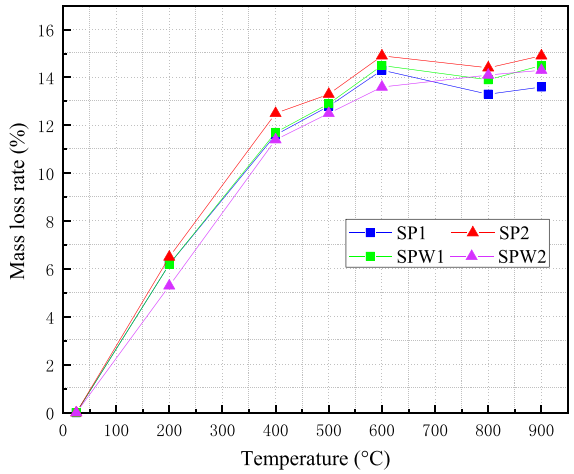

Fig. 11 Mass loss rate after exposure to different temperatures

exposed to 600 °C. Above 600 °C, SPW1 and SPW2 still had the higher relative UPV compared to SP1 and SP2 even though CW seriously deteriorated, which may attributed to the formation of ceramic phases.

Figure 11 shows the mass loss rate of HFRCCs after exposure to elevated temperatures. The mass loss rate increased with the increase of temperature. For this phenomenon, the main reason was the evaporation of free water in the capillary pores and dehydration of C–S–H, AFt and AFm, melting of PVA fibers, decomposition of $Ca(OH)_2$, $CaCO_3$ and C–S–H.

3.5 SEM observation

In order to investigate the internal deterioration mechanism of HFRCCs after exposure to high temperatures, SEM observation was carried out and shown in Fig. 12.

The reinforcing effect of CW can be explained by micro-mechanical mechanisms in terms of whisker bridging, whisker breakage, crack deflection, and whisker pull-out. Bridging is commonly believed to be a reinforcing mechanism for fiber reinforced cementitious composites [41]. As shown in Fig. 12(b), CW bridged the cracks and thus improved the flexural and tensile performance of SPW1 and SPW2. Moreover, steel fiber, PVA fiber and CW demonstrated reinforcing effect at different scales shown in (a), (b) and (c) below 200 °C. Between 200 and 400 °C, PVA fibers were no longer observed lost the ability to limit the development of cracks and introduced new pores into the matrix (shown in (d)). As a result, the residual flexural strengths, splitting tensile strengths and UPV deteriorated. In Fig. 12e, CW was embedded

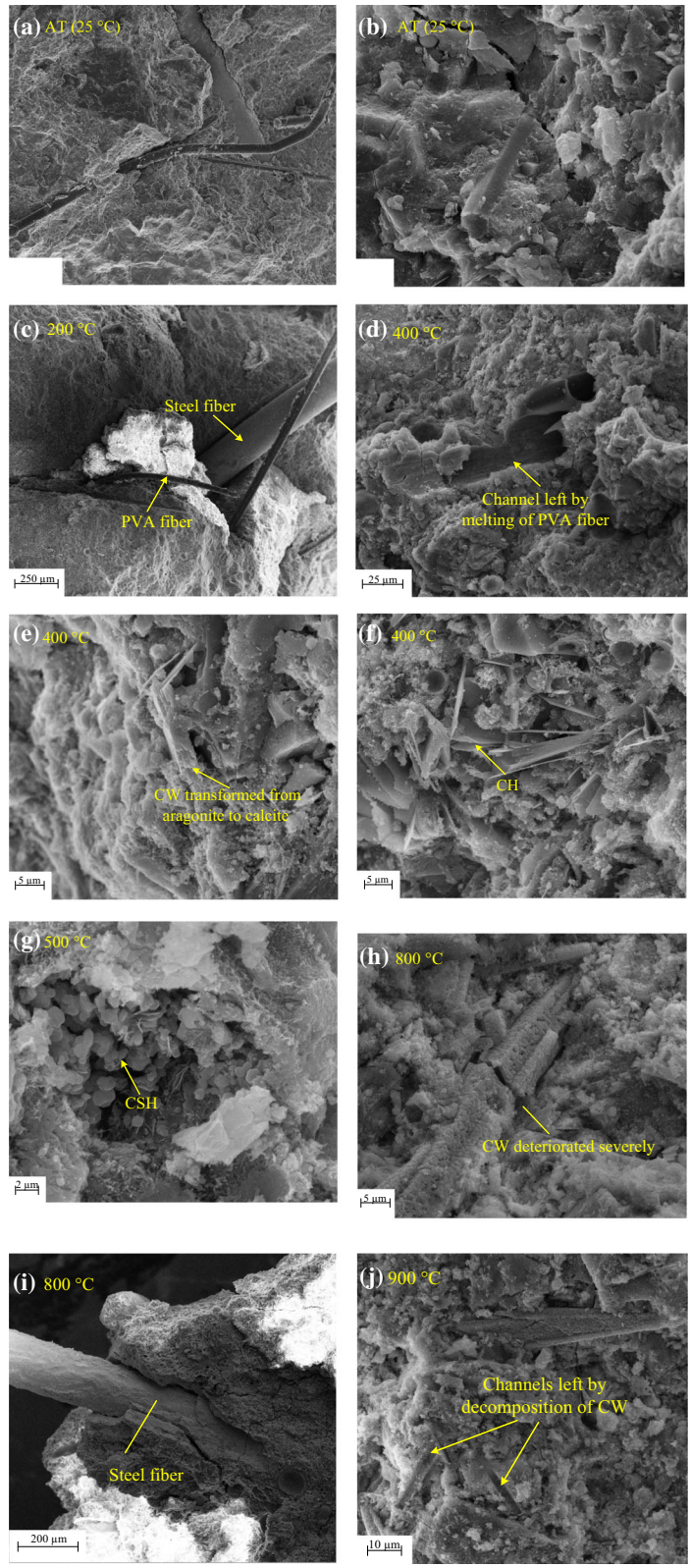

Fig. 12 Micro-morphologies of HFRCCs after exposed to different temperatures. *Notes*: C–S–H gels were marked with "CSH", $Ca(OH)_2$ crystals were marked with "CH"

in matrix and attached by many hydration products, which proved the nucleation effect of calcite CW after exposed to 400 °C [11, 35, 36]. Therefore, the compressive strengths of HFRCCs containing CW increased from 200 to 400 °C. In Fig. 12f and g, The $Ca(OH)_2$ began to decompose and lost its regular shape, thus led to further loss of mass and reduction in strengths. At around 800 °C (see in (h)), CW was seriously deteriorated by elevated temperatures and thus caused further decrease of UPV and increase of mass loss rates. Figure 12i showed the microstructure of steel fiber in matrix at 800 °C. The surface attachment showed that the steel fiber was well bonded with the matrix. In the whole high temperature range, compared with CW and PVA fibers, steel fibers played a more significant role in strengthening the strength of HFRCCs. After exposure to 900 °C, the channels left by decomposition of CW and microscopic morphology of HFRCCs are showed in Fig. 12j. CW were completely decomposed and lost its reinforcing effect.

4 Conclusion

The mechanical and physical responses of HFRCCs after exposure to high temperature were systematically studied and the role of multi-scale fiber systems were revealed by SEM observation. The conclusions can be drawn as follows:

(1) The residual flexural and splitting tensile strengths of HFRCCs decreased with the increase of temperatures. This attribute to the dehydration of hydration products, melting of PVA fibers, decomposition of $Ca(OH)_2$ and $CaCO_3$. Particularly, the compressive strengths increased from 200 to 400 °C because of the reinforcing effect of CW and further hydration of unhydrated cement particles.

(2) HFRCCs showed better hardening responses and post-peak softening branches below 200 °C than those above 200 °C. PVA fiber was effective improve the ability of HFRCCs to bear external loads after exposure to high temperature until it melt.

(3) Generally, the UPV decreased with the increase of temperature, and the mass loss rate increased at the whole heating process.

(4) Through the SEM observation, it can be found PVA fibers melt above 200 °C and deteriorated the flexural and splitting tensile strengths. CW demonstrated nucleation effect to improve the compressive strengths at around 400 °C. Generally, steel fibers were most effective to reduce the strength and microstructure deterioration of HFRCCs at the whole heating process because of their highest thermostability and favorable bond strength with matrix.

Acknowledgements The authors acknowledge the support of the Natural Science Foundation of China under Grant No. 51678111 and No. 51478082.

References

1. Yoo D-Y, Banthia N, Yang J-M, Yoon Y-S (2016) Size effect in normal- and high-strength amorphous metallic and steel fiber reinforced concrete beams. Constr Build Mater 121:676–685
2. Cao M, Zhang C, Lv H, Xu L (2014) Characterization of mechanical behavior and mechanism of calcium carbonate whisker-reinforced cement mortar. Constr Build Mater 66:89–97
3. Cao M, Li L, Zhang C, Feng J (2018) Behaviour and damage assessment of a new hybrid-fibre-reinforced mortar under impact load. Mag Concrete Res 70:905–918
4. Cao M, Li L, Yin H, Ming X (2019) Microstructure and strength of calcium carbonate ($CaCO_3$) whisker reinforced cement paste after exposed to high temperatures. Fire Technol 55(6):1983–2003
5. Banthia N, Soleimani S (2015) Flexural response of hybrid fiber-reinforced cementitious composites. ACI Mater J 102(6):382–389
6. Kang S-T, Choi J-I, Koh K-T, Lee KS, Lee BY (2016) Hybrid effects of steel fiber and microfiber on the tensile behavior of ultra-high performance concrete. Compos Struct 145:37–42
7. Cao M, Zhang C, Li Y, Wei J (2015) Using calcium carbonate whisker in hybrid fiber-reinforced cementitious composites. ASCE J Mater Civ Eng 27(4):04014139
8. Kwon S, Nishiwaki T, Kikuta T, Mihashi H (2014) Development of ultra-high-performance hybrid fiber reinforced cement-based composites. ACI Mater J 111(3):309–318
9. Han T, Wang H, Jin X, Yang J, Lei Y, Yang F et al (2014) Multiscale carbon nanosphere–carbon fiber reinforcement for cement-based composites with enhanced high-temperature resistance. J Mater Sci 50(5):2038–2048
10. Du Q, Wei J, Lv J (2018) Effects of high temperature on mechanical properties of polyvinyl alcohol engineered cementitious composites (PVA-ECC). Int J Civ Eng 16(8):965–972
11. Li L, Cao M, Ming X, Yin H, Sun YN (2019) Microstructure of calcium carbonate whisker reinforced cement paste after

elevated temperature exposure. Constr Build Mater 227:116609
12. Konsta-Gdoutos MS, Metaxa ZS, Shah SP (2010) Highly dispersed carbon nanotube reinforced cement based materials. Cem Concr Res 40:1052–1059
13. Materazzi AL, Ubertini F, D'alessandro A (2013) Carbon nanotube cement-based transducers for dynamic sensing of strain. Cem Concr Compos 37:2–11
14. Han B, Yang Z, Shi X, Yu X (2013) Transport properties of carbonnanotube/cement composites. J Mater Eng Perform 22(1):184–189
15. Li GY, Wang PM, Zhao X (2005) Mechanical behavior and microstructure of cement composites incorporating surface-treated multi-walled carbon nanotubes. Carbon 43(6):1239–1245
16. Florence S, Chantal I (2009) Microstructure and macroscopic properties of hybrid carbon nanofiber/silica fume cement composites. Compos Sci Technol 69(7):1310–1318
17. Siddique R, Mehta A (2014) Effect of carbon nanotubes on properties of cement mortars. Constr Build Mater 50:116–129
18. Gales J, Parker T, Cree D, Green M (2016) Fire performance of sustainable recycled concrete aggregates: mechanical properties at elevated temperatures and current research needs. Fire Technol 52:817–845
19. Ma Q, Guo R, Zhao Z, Lin Z, He K (2015) Mechanical properties of concrete at high temperature: a review. Constr Build Mater 93:371–383
20. Abid M, Hou X, Zheng W, Hussain RR (2017) High temperature and residual properties of reactive powder concrete—a review. Constr Build Mater 147:339–351
21. Piasta J, Sawicz Z, Rudzinski L (1984) Changes in the structure of hardened cement paste due to high temperature. Mater Constr 17:291–296
22. Zhang C, Cao M (2014) Fiber synergy in multi-scale fiber-reinforced cementitious composites. J Reinf Plast Compos 33(9):862–874
23. Cao M, Li L, Khan M (2018) Effect of hybrid fibers, calcium carbonate whisker and coarse sand on mechanical properties of cement-based composites. Mater Constr 68(330):e156
24. Pan J, Cai J, Ma H, Leung CKY (2018) Development of multiscale fiber-reinforced engineered cementitious composites with PVA fiber and $CaCO_3$ whisker. J Mater Civ Eng 30(6):04018106
25. Chinese National Standard. GB/T 50081 (2002) Standard for test method of mechanical properties on ordinary concrete. China. (**in Chinese**)
26. Cao M, Ming X, Yin H, Li L (2019) Influence of high temperature on strength, ultrasonic velocity and mass loss of calcium carbonate whisker reinforced cement paste. Compos B Eng 163:438–446
27. Standard ASTM (2016) Standard test method for pulse velocity through concrete, ASTM Standard C597-16. ASTM International, West Conshohocken
28. CECS Standard (2000) Technical specification for inspection of concrete defects by ultrasonic method. CECS 21:2000, Beijing, P.R. China. (**in Chinese**)
29. Sahmaran M, Lachemi M, Li V (2010) Assessing mechanical properties and microstructure of fire-damaged engineered cementitious composites. ACI Mater J 107(3):297–304
30. Liu J-C, Tan KH (2017) Fire resistance of strain hardening cementitious composite with hybrid PVA and steel fibers. Constr Build Mater 135:600–611
31. Morsy M, Galal A, Abo-El-Enein S (1998) Effect of temperature on phase composition and microstructure of artificial pozzolana-cement pastes containing burnt kaolinite clay. Cement Concr Res 28(8):1157–1163
32. Villain G, Thiery M, Platret G (2007) Measurement methods of carbonation profiles in concrete: thermogravimetry, chemical analysis and gammadensimetry. Cement Concr Res 37(8):1182–1192
33. Xing Z, Beaucour A-L, Hebert R, Noumowe A, Ledesert B (2011) Influence of the nature of aggregates on the behaviour of concrete subjected to elevated temperature. Cement Concr Res 41(4):392–402
34. Akca AH, Özyurt Zihnioğlu N (2013) High performance concrete under elevated temperatures. Constr Build Mater 44:317–328
35. Bentz DP, Ardani A, Barrett T, Jones SZ, Lootens D, Peltz MA et al (2015) Multi-scale investigation of the performance of limestone in concrete. Constr Build Mater 75:1–10
36. Li L, Cao M, Yin H (2019) Comparative roles between aragonite and calcite calcium carbonate whiskers in the hydration and strength of cement paste. Cement Concr Compos 104:103350
37. Peng G-F, Huang Z-S (2008) Change in microstructure of hardened cement paste subjected to elevated temperatures. Constr Build Mater 22(4):593–599
38. Lin W-M, Lin TD, Powers-Couche LJ (1996) Microstructures of fire-damaged concrete. ACI Mater J 93(3):199–205
39. JCI-SF4 (1983) Methods of tests for flexural strength and flexural toughness of fiber reinforced concrete, JCI Standards for Test Methods of Fiber Reinforced Concrete, Japan Concrete Institute, Japan, 1983, pp 45–51
40. Pourfalah S (2018) Behaviour of engineered cementitious composites and hybrid engineered cementitious composites at high temperatures. Constr Build Mater 158:921–937
41. Cao M, Xu L, Zhang C (2016) Rheology, fiber distribution and mechanical properties of calcium carbonate ($CaCO_3$) whisker reinforced cement mortar. Compos A Appl Sci Manuf 90:662–669